

**Structure and kinetics of a transient antibody binding intermediate reveal a kinetic discrimination mechanism in antigen recognition**

Leo C. James, and Dan S. Tawfik

*PNAS* 2005;102;12730-12735; originally published online Aug 29, 2005;  
doi:10.1073/pnas.0500909102**This information is current as of November 2006.**

<b>Online Information &amp; Services</b>	High-resolution figures, a citation map, links to PubMed and Google Scholar, etc., can be found at: <a href="http://www.pnas.org/cgi/content/full/102/36/12730">www.pnas.org/cgi/content/full/102/36/12730</a>
<b>Supplementary Material</b>	Supplementary material can be found at: <a href="http://www.pnas.org/cgi/content/full/0500909102/DC1">www.pnas.org/cgi/content/full/0500909102/DC1</a>
<b>References</b>	This article cites 26 articles, 12 of which you can access for free at: <a href="http://www.pnas.org/cgi/content/full/102/36/12730#BIBL">www.pnas.org/cgi/content/full/102/36/12730#BIBL</a>  This article has been cited by other articles: <a href="http://www.pnas.org/cgi/content/full/102/36/12730#otherarticles">www.pnas.org/cgi/content/full/102/36/12730#otherarticles</a>
<b>E-mail Alerts</b>	Receive free email alerts when new articles cite this article - sign up in the box at the top right corner of the article or <a href="#">click here</a> .
<b>Rights &amp; Permissions</b>	To reproduce this article in part (figures, tables) or in entirety, see: <a href="http://www.pnas.org/misc/rightperm.shtml">www.pnas.org/misc/rightperm.shtml</a>
<b>Reprints</b>	To order reprints, see: <a href="http://www.pnas.org/misc/reprints.shtml">www.pnas.org/misc/reprints.shtml</a>

Notes:

# Structure and kinetics of a transient antibody binding intermediate reveal a kinetic discrimination mechanism in antigen recognition

Leo C. James<sup>\*†</sup> and Dan S. Tawfik<sup>†‡</sup>

<sup>\*</sup>Laboratory of Molecular Biology, Medical Research Council, Cambridge CB2 2HQ, United Kingdom; and <sup>†</sup>Department of Biological Chemistry, Weizmann Institute of Science, Rehovot 76 100, Israel

Edited by Herman N. Eisen, Massachusetts Institute of Technology, Cambridge, MA, and approved July 21, 2005 (received for review February 4, 2005)

**Induced fit is a predominant phenomenon in protein–ligand interactions, yet it is invariably attributed without establishing the existence, let alone the structure, of the initial, low-affinity encounter complex. We determined the crystal structure of the encounter complex on the pathway of ligand binding by IgE antibody SPE7. We show that this complex is formed by a wide range of ligands that initially bind with identical affinity. Nonspecific ligands rapidly dissociate, whereupon the antibody isomerizes to a nonbinding isomer. Specific ligand complexes, however, slowly isomerize to give a high-affinity complex. This isomerization involves backbone and side-chain rearrangements of up to 14 Å and the formation of specific hydrogen bonds. The postbinding conformational switch, combined with the prebinding isomerization to an energetically favorable nonbinding isomer, results in a “kinetic discrimination” mechanism that mediates selective binding, by a factor of  $>10^3$ , between highly related ligands that initially bind with the same affinity. This model may apply to proteins that bind multiple ligands in a specific manner or other proteins that, although capable of binding many ligands, are activated by only a few.**

conformational diversity | induced fit | multispecificity | promiscuity

**M**any biological systems include proteins that bind multiple ligands in a selective manner. In the immune system, a single T cell antigen receptor recognizes up to  $10^5$  different peptides yet differentiates highly related sequences into agonists or antagonists (1). In cell-cycle regulation, one kinase inhibitor can specifically bind a number of different cyclin-Cdk complexes (2). In G protein-coupled receptors, both agonists and antagonists bind the receptor, but only agonists result in productive signaling (3). Although the detailed mechanism of each of the systems described above is yet to be determined, protein dynamics seems to play a key role in all of them (4).

The classical view of protein structure and function is that proteins act like switches through changes in conformation that are induced after binding or activation. However, there is growing evidence that these switches involve a population shift between existing protein conformations. The ability to adopt multiple conformations has also been associated with the ability to bind multiple ligands (1, 5, 6). We recently demonstrated the ability of a single protein, the IgE antibody SPE7, to bind two completely unrelated ligands through two different pre-existing conformations (7). One conformation (dubbed Ab<sup>2</sup>), which is 20% populated, has a deep and narrow binding site that binds the immunizing hapten [dinitrophenol (DNP), a small aromatic compound]. The other conformation (Ab<sup>1</sup>) is 80% populated, has a flat binding surface, and binds a promiscuous protein antigen (7).

Conformational diversity also links structural changes (local or even folding of an entire domain or protein) with function. Ligands binding a scarcely populated, high-energy conformation will not shift the equilibrium toward the complexed state unless they make sufficient contacts to stabilize it over other more energetically stable free forms. This principle seems to be borne out *in vivo*. The

intrinsic disorder of many DNA-binding proteins is thought to reduce binding to nonspecific sequences (8). In the G protein-coupled receptor  $\beta_2$ -adrenergic receptor, there is evidence that the agonist-binding pocket is not preformed but is dynamically assembled as the ligand binds (9). An active site that only partially exists before complexation was also identified in the *Tetrahymena* ribozyme (10).

The immune response faces the challenge of recognizing a large number of different molecules while maintaining specificity and differentiating between very closely related homologues. In the IgE antibody SPE7, both cross-reactivity and exquisite specificity exist side by side. In addition to binding the immunizing hapten (DNP), SPE7 isomer Ab<sup>2</sup> binds to a number of other synthetic ligands, including furazolidone and three-ring quinones (11). Interestingly, although SPE7 accommodates these quite different compounds, it is able to discriminate between highly related derivatives (12). For instance, the quinone anthraflavic acid differs from alizarin in the position of a single hydroxyl but binds with  $>1,000$ -fold lower affinity (Table 1). We have examined how SPE7 accomplishes multispecificity and selectivity within a single binding site and how its conformational dynamism mediates this ability.

We show that binding of anthrone and anthraflavic acid, which is barely detectable at equilibrium ( $K_a < 10^4 \text{ M}^{-1}$ ; Table 1), initially follows the same pre-steady-state binding kinetics as the high-affinity ligands for SPE7. In fact, both specific and nonspecific ligands form a transient antibody complex with identical affinity. The structure of this low-affinity encounter complex ( $K_a \approx 10^5 \text{ M}^{-1}$ ) is presented here. Specific ligands (e.g., DNP-Ser or alizarin) are capable of “locking-in” the antibody into a second, rearranged, high-affinity conformation, Ab<sup>3</sup> (7). This locking-in is the result of a few highly selective hydrogen bonds made solely by specific ligands with residues that become exposed only in the Ab<sup>3</sup> conformation. This isomerization, combined with a pre-equilibrium isomerization between Ab<sup>2</sup> and a more stable nonhapten-binding free isomer (Ab<sup>1</sup>) result in a “kinetic discrimination” mechanism that enables SPE7 to distinguish, by a factor of  $>1,000$ , between highly related ligands that initially bind with the same affinity.

## Materials and Methods

**Pre-Steady-State Kinetics.** Kinetics were followed with an Applied Photophysics (Surrey, U.K.) stopped-flow instrument at 20°C using purified ( $>99\%$ ) SPE7 Fv between 0.1 and 1  $\mu\text{M}$  in PBS (pH 7.4) (7). Samples were excited at 280 nm, and emission was monitored through a 320-nm-cutoff filter. Ligands were dissolved in DMSO at 50 mM and freshly diluted into PBS with extensive vortexing to

This paper was submitted directly (Track II) to the PNAS office.

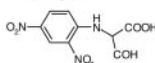
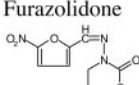
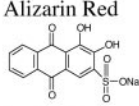
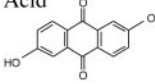
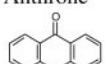
Abbreviations: DNP, dinitrophenol; CDR, complementarity-determining region.

Data deposition: The atomic coordinates and structure factors have been deposited in the Protein Data Bank, [www.pdb.org](http://www.pdb.org) (PDB ID code 2BJM).

<sup>†</sup>To whom correspondence may be addressed. E-mail: [tawfik@weizmann.ac.il](mailto:tawfik@weizmann.ac.il) or [lcj@mrc-lmb.cam.ac.uk](mailto:lcj@mrc-lmb.cam.ac.uk).

© 2005 by The National Academy of Sciences of the USA

Table 1. Summary of the kinetic and equilibrium constants for SPE7 binding

Ligand	Pre-equilibrium				Binding to Ab <sup>2</sup>			Induced fit			
	$K_a, M^{-1}$ <sup>a</sup>	$k_1, s^{-1}$	$k_{-1}, s^{-1}$	$K_1$	$k_2, M^{-1}s^{-1}$	$k_{-2}, s^{-1}$	$K_2, M^{-1}$	$k_3 + k_{-3}, s^{-1}$	$k_{3,S}^{-1†}$	$k_{-3,S}^{-1†}$	$K_3^{\ddagger}$
DNP-Ser 	$(0.5 \pm 0.07) \times 10^8$	$17 \pm 1$	$58 \pm 2.5$	$0.29 \pm 0.04$	$(9.5 \pm 0.5) \times 10^6$	$96 \pm 20$	$(1 \pm 0.26) \times 10^5$	$1.9 \pm 0.2$	1.9	$1 \times 10^{-3}$	$1.7 \times 10^3$
Furazolidone 	$(0.83 \pm 0.07) \times 10^6$	$14 \pm 0.75$	$55 \pm 3.4$	$0.25 \pm 0.03$	$(6 \pm 0.14) \times 10^6$	$66 \pm 6$	$(0.91 \pm 0.33) \times 10^5$	$0.8 \pm 0.3$	0.8	$2 \times 10^{-2}$	$3.6 \times 10$
Alizarin Red 	$(0.22 \pm 0.05) \times 10^8$	$17 \pm 3.4$	$61 \pm 1.6$	$0.28 \pm 0.06$	$(3.4 \pm 0.24) \times 10^6$	$126 \pm 13$	$(0.27 \pm 0.05) \times 10^5$	$1.8 \pm 0.3$	1.8	$6 \times 10^{-4}$	$2.9 \times 10^3$
Anthraflavic Acid 	$< 10^{49}$	$6.5 \pm 2.5$	$53 \pm 2.4$	$0.31 \pm 0.05$	$(3.6 \pm 0.6) \times 10^6$	$73 \pm 10$	$(2 \pm 0.25) \times 10^5$				
Anthrone 	$< 10^{49}$	ND	ND	ND	$(4.7 \pm 0.18) \times 10^6$	$45 \pm 4$	$(1.04 \pm 0.31) \times 10^5$				

<sup>a</sup>Association constants ( $K_a$ ) were measured at equilibrium by using fluorescence quenching (see *Materials and Methods*).

<sup>†</sup>The "on" and "off" rates of isomerization ( $k_3$ , and  $k_{-3}$ , respectively) were not measured directly but deduced from the measured rate constants of isomerization, assuming that, for a unimolecular isomerization,  $1/\tau = k_3 + k_{-3}$  (15), and that  $k_3/k_{-3} = K_3$ .

<sup>‡</sup>The association constant of the final, induced-fit isomerization step ( $K_3$ ) was not measured directly but deduced from SPE7's overall affinity constant at equilibrium ( $K_a$ ), assuming that  $K_a = K_1 \times K_2 \times K_3$  (15).

<sup>††</sup>The affinity at equilibrium was assessed by competitive ELISA against a low-affinity DNA analogue immobilized onto a carrier protein.

ensure that no precipitation occurred. Data from three or more independent measurements were averaged for each concentration of ligand. Each phase was generally observed for at least 10 half-lives, and its trace was fitted to a single exponential ( $F_t = F_0 \exp[-(1/\tau)t] + F_\infty$ , where  $F_t$  is the fluorescence (in arbitrary units) at time  $t$ ;  $F_\infty$  is the fluorescence at  $t = \infty$ ,  $1/\tau$  is the reciprocal relaxation time ( $k_{obs}$ ) and  $F_0$  is the amplitude ( $F_\infty$  minus fluorescence at  $t = 0$ )). Fits of data corresponding to two phases were performed with  $\{F_t = F_1 \exp[-(1/\tau_1)t] + F_2 \exp[-(1/\tau_2)t] + F_\infty\}$  and fits of data corresponding to three phases to Eq. 3  $\{F_t = F_1 \exp[-(1/\tau_1)t] + F_2 \exp[-(1/\tau_2)t] + F_3 \exp[-(1/\tau_3)t] + F_\infty\}$ . Anthrone and anthraflavic acid both gave biphasic kinetics, although the second (pre-equilibrium) phase was barely visible with anthrone. The pre-equilibrium phase was generally much clearer with the high-affinity ligands (7) than in the low-affinity ligands used here. There are a number of reasons for this result. First, the quality of data for the low-affinity ligands was generally poorer. Second, the proportion of bound antibody at the end of the experiment was lower; thus, the concentration of free Ab<sup>2</sup> does not change to the same extent as with the higher-affinity ligands. Given a  $K_d$  of  $\approx 200 \mu M$  (anthrone; Table 1), an antibody concentration of  $0.1 \mu M$ , and a ligand concentration of  $20 \mu M$ , the percentage of bound antibody is  $< 9\%$ ; consequently, the shift in the fraction of Ab<sup>1</sup> toward Ab<sup>2</sup> (the change to which the pre-equilibrium phase corresponds) is minor ( $< 7.2\%$ ), and the fluorescence change difficult to detect.

**X-Ray Crystallography.** Freshly purified SPE7 Fv was exchanged into 10 mM Hepes (pH 7.0)/20 mM NaCl. Crystals were grown by the hanging-drop method. Similar to the structure of free isomer Ab<sup>2</sup>, the anthrone complex has apparent I422 symmetry. However, the average  $\langle I^2 \rangle / \langle I \rangle^2$  is 1.77 for all reflections (with a minimum of 1.49 for the 302 reflections in the resolution range of 4.7–4.62 Å), which

is indicative of twinning. The sigmoidal nature of the acentric cumulative intensity distribution also suggested twinning. The actual space group of the anthrone complex is I4 with one copy per asymmetric unit and twinning providing the apparent additional twofold diagonal symmetry. Attempts at molecular replacement also highlighted the twinned nature of the data: no solution was found for I422, but replacement in I4 gave a strong solution. Iterative rounds of refinement in REFMAC with detwinning in CNS resulted in a model with an  $R$  factor of 0.27. Statistics for data collection and refinement are given in Table 2. Density was complete, including for the ligand anthrone. An omit map for the ligand is shown in Fig. 5, which is published as supporting information on the PNAS web site. Additional evidence that the anthrone complex is similar to Ab<sup>2</sup>, not to Ab<sup>1</sup> or Ab<sup>3</sup>, is provided by crystal-packing constraints. The complementarity-determining region (CDR) H3 loops from these structures when brought into

Table 2. Refinement statistics for the anthrone–SPE7 complex

Space group	I4
Cell	$a = 79.7; b = 79.7; c = 67.9$
Number of copies	1
Resolution, Å	2.15
Unique reflections	11,641
$R_{merge}$	0.064 (0.210)
Redundancy	4.1
Completeness, %	99.9 (99.9)
Average $I/\sigma I$	11.4 (4.4)
Final $R_{cryst}$	0.27
Final $R_{free}$	0.29
Bond/angle rms deviation	0.005/1.2°

Numbers in parentheses are for the highest-resolution shell.

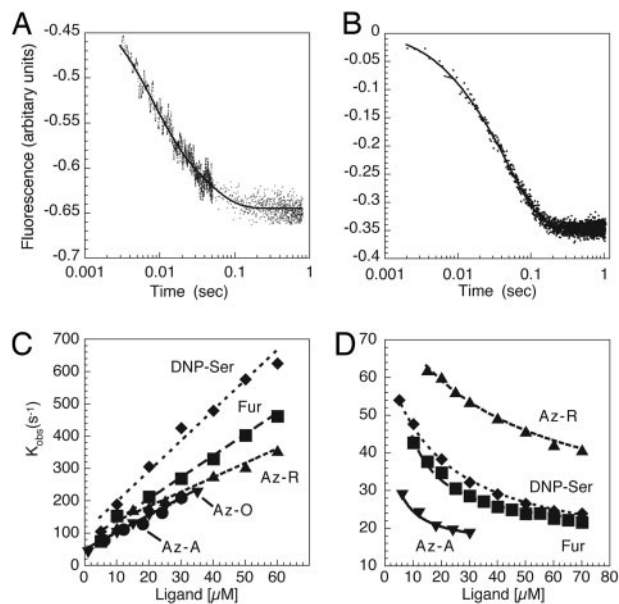
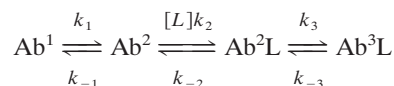


**Fig. 1.** Pre-steady-state kinetics of SPE7 complexation. (A and B) Fluorescence quenching traces observed after mixing with 50  $\mu\text{M}$  anthrone (A) or 30  $\mu\text{M}$  anthraflavic (B) are shown. The plots were fitted to a double exponential, with a fast phase (0.001 and 0.03 s) and a second phase (0.03 and 0.3 s). Rate constants for these steps were derived by fitting each phase to a single exponential. (C) Rates of the fast phase as a function of ligand concentration. The rates for each ligand concentration were fitted to a bimolecular association model ( $\text{Ab}^2 + \text{L} \leftrightarrow \text{Ab}^2\text{L}$ ) by using Eq. 1. (D) Rates of the second phase as a function of ligand concentration fitted to a pre-equilibrium model ( $\text{Ab}^1 \leftrightarrow \text{Ab}^2$ ) by using Eq. 2.

the I4 cell produce multiple main-chain clashes. The final model was validated by using the program PROCHECK (13). Surface complementation scores were calculated by using the CCP4 program SC (13). Figures were prepared by using PYMOL (14). Morph movies were created by generating restrained intermediates using the development version of the MORPH SERVER ([www.molmovdb.org/cgi-bin/multichain.cgi](http://www.molmovdb.org/cgi-bin/multichain.cgi)), creating surfaces in PYMOL, and animating the stills in Adobe IMAGEREADY 7.

## Results

**Pre-Steady-State Kinetics.** The pre-steady-state binding kinetics of SPE7 were determined by monitoring, in a stopped-flow apparatus, the quenching of intrinsic tryptophan fluorescence after ligand binding as a function of time. The rates followed one exponential phase for anthrone (Fig. 1A) and two phases for anthraflavic acid (Fig. 1B). Because the two phases occurred over distinct time scales (a fast phase of  $<0.1$  s and a slower phase between 0.03 and 1 s), they were separated and fitted individually to a single exponential. The relaxation times ( $\tau$ ) were determined for each phase, and the corresponding rate constants were derived ( $k_{\text{obs}} = 1/\tau$ ) assuming pseudo-first-order conditions ( $[\text{antibody}] \leq 10 \times [\text{ligand}]$ ). The full data set for the entire time range at each concentration was also fitted to a double exponential (Fig. 1B) to verify that no bias was introduced by fitting the phases separately. Rate constants were determined by plotting the relaxation times over a range of ligand concentrations (Fig. 1C and D). Because the hydrophobicity of the ligands limited their solubility, pseudo-first-order conditions were maintained by decreasing the antibody concentration (0.1  $\mu\text{M}$ ). Although this led to a decrease in signal-to-noise ratio relative to the experiments performed with high-affinity ligands (7), the data were of good quality and could be readily fitted with low error (fits of individual phases to one exponential gave an  $R$  value of  $\geq 0.98$ ). The observed binding kinetics are unlikely to be the result of exchange



**Scheme 1.**

between the two chains of the Fv, because previous results with high-affinity ligands were found to be the same with both the intact antibody and the Fv (7).

**The First Phase Corresponds to a Bimolecular Association.** The observed rate of the fast phase exhibits a linear dependency on ligand concentration (Fig. 1) that is consistent with a simple bimolecular association of antibody with ligand (Scheme 1; middle step) as modeled in Eq. 1 (15, 16):

$$1/\tau_1 = k_{\text{obs}} = k_{-2} + k_2[L]. \quad [1]$$

Fits to Eq. 1 gave very similar “on” and “off” rate constants for anthraflavic acid and anthrone ( $k_2$  and  $k_{-2}$ , respectively; Table 1).

**The Second Phase Corresponds to a Pre-Equilibrium Between Two Antibody Isomers.** The observed rate of the second phase decreases with ligand concentration (Fig. 1D), which is consistent with an equilibrium between two pre-existing antibody conformers, only one of which binds the ligand (Scheme 1; first step), and was fitted to a “pre-equilibrium” model by using Eq. 2:

$$1/\tau_2 = k_{\text{obs}} = k_1 + k_{-1}(K_2/([L] + K_2)). \quad [2]$$

This fit, when applied to the anthraflavic acid data gave the following parameters:  $k_1 = 16.5 \text{ s}^{-1}$ ,  $k_{-1} = 53 \text{ s}^{-1}$ , and  $K_2 = 2 \times 10^{-5} \text{ M}^{-1}$  (Fig. 1; Table 1). The value of  $K_2$  is only 2-fold higher than the affinity constant that is derived from the independent measurements of the fast phase ( $K_2 = k_2/k_{-2}$ ; Table 1). In addition, when the value of  $K_2$  obtained from the fit of the fast (first) phase to Eq. 1 is introduced into Eq. 2, values close to the error range for  $k_1$  and  $k_{-1}$  were obtained. Because the rate of this phase decreases with increasing ligand concentration while the rate of the first phase increases, the two phases are best separated at higher ligand ratios. Unfortunately, the very low solubility of anthrone and its slightly lower affinity did not allow us to collect enough data to determine the rate constants of the second phase. Nevertheless, the kinetic model and rate constants for anthrone and anthraflavic acid support a mechanism in which these nonspecific ligands bind a lesser-populated ( $\approx 20\%$ ) isomer  $\text{Ab}^2$  to give an encounter complex that, although formed with a rapid on rate ( $k_2 \approx 10^6 \text{ M}^{-1}\text{s}^{-1}$ ), also dissociates very rapidly ( $k_{-2} > 50 \text{ s}^{-1}$ , corresponding to a dissociation half-life of  $<15$  ms). The result is a low-affinity encounter complex with an affinity constant ( $K_2$ ) of  $\approx 10^5 \text{ M}^{-1}$ .

The first two steps described in Scheme 1 are also present in the binding of the immunizing hapten, DNP-Ser, and high-affinity cross-reactants such as furazolidone and alizarin red (7). Comparison of the rate constants reveals that all ligands, low and high affinity alike, bind  $\text{Ab}^2$  with similar rates and affinity (Table 1). The free isomer  $\text{Ab}^2$  is therefore highly promiscuous, indiscriminately binding many aromatic ligands with the same affinity. The barely detectable binding of anthrone and anthraflavic at equilibrium is not only the result of low affinity to  $\text{Ab}^2$  ( $K_2 \approx 10^5 \text{ M}^{-1}$ ) but also of its relative instability.  $\text{Ab}^2$  rapidly converts to a nonbinding energetically dominant isomer  $\text{Ab}^1$  (7). Binding of ligand to  $\text{Ab}^2$  therefore competes with isomerization to  $\text{Ab}^1$ . Based on the kinetic rate constants of the pre-equilibrium and bimolecular association steps, the calculated affinity of the ligand- $\text{Ab}^2$  complex is  $K_1 \times K_2 \approx 3 \times 10^4 \text{ M}^{-1}$ . This value is similar to the measured equilibrium affinities of nonspecific ligands anthrone and anthraflavic acid

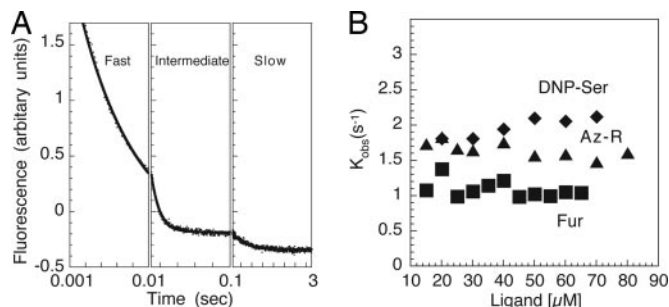


**Fig. 2.** Pre-steady-state kinetics of SPE7 complexation with specific ligands. (A) Fluorescence quenching trace observed after mixing with 20  $\mu\text{M}$  alizarin red. The three discrete phases are marked and shown as split abscissa: fast (0.001–0.02 s), intermediate (0.02–0.2 s), and slow (0.2–3 s). These phases were separated and each fitted to a single exponential to derive the rate constants for each step. (B) The reciprocal relaxation times of the slow phase as a function of ligand concentration.

(Table 1). A question remains, however: how is SPE7 capable of binding DNP-Ser and alizarin red with an equilibrium affinity of  $\approx 10^8 \text{ M}^{-1}$  when it initially binds them at  $3 \times 10^4 \text{ M}^{-1}$ .

**The Origin of Ligand Discrimination in SPE7.** The pre-equilibrium kinetics with the high-affinity ligands exhibit a third phase that is entirely absent in anthraflavic acid and anthrone (Fig. 2A). This phase is slower than both the bimolecular association and isomerization steps and exhibits almost no dependency on ligand concentration (Fig. 2B). We previously ascribed this phase to an induced-fit isomerization of the low-affinity complex to a high-affinity complex (Scheme 1;  $\text{Ab}^2\text{-L} \leftrightarrow \text{Ab}^3\text{-L}$ ) (7). Because the amplitude for this step is small and its rate is unimolecular and kinetically detached from the other, ligand-dependent steps, the kinetic constants ( $k_3$ ,  $k_{-3}$ ) cannot be measured directly, although their magnitude can be derived from the data. The affinity constant ( $K_3$ ) can be derived from the equilibrium affinity constant ( $K_a$ ) and the microscopic affinity constants ( $K_1$  and  $K_2$ ) assuming that  $K_a = K_1 \times K_2 \times K_3$ . Values for the rate constants  $k_3$  and  $k_{-3}$  can be extrapolated also. Because the reverse rate must be much slower than the forward rate ( $k_{-3} \ll k_3$ ), the reciprocal relaxation time,  $1/\tau$  or  $k_{\text{obs}}$ , is essentially a function of the forward rate ( $1/\tau = k_{-3} + k_3 \approx k_3$ ). The reverse rate ( $k_{-3}$ ) is then simply  $k_3/K_3$ . As can be seen in Table 1, the final isomerization to  $\text{Ab}^3$  increases the affinity of specific ligands (e.g., alizarin red and DNP-Ser) by  $>1,000$ -fold. Thus, the ability of SPE7 to discriminate between specific and nonspecific ligands depends on a postbinding isomerization of a

low-affinity encounter complex ( $\text{Ab}^2\text{-L}$ ) to a high-affinity complex ( $\text{Ab}^3\text{-L}$ ).

**Structure of the Low-Affinity Encounter Complex with Anthrone.** Our model suggests that both specific and nonspecific ligands bind to the same free isomer ( $\text{Ab}^2$ ) to yield an essentially identical encounter complex ( $\text{Ab}^2\text{-L}$ ) with no significant structural rearrangements relative to the free antibody. The fact that all SPE7 ligands form the same encounter complex is confirmed by the kinetics, which show that in each case the measured equilibrium binding constant for the initial encounter complex is the same. Because of their highly transient nature, the structures of encounter complexes can only be deduced from the structures of the free (uncomplexed) protein. However, because SPE7 ligands such as anthrone do not proceed to the final, high-affinity complex, they provide a unique opportunity to solve the structure of the transient encounter complex.

We previously solved two crystal structures of free SPE7 and several high-affinity complexes with different specific ligands ( $\text{Ab}^3\text{-L}$ ). One of the free isomers (dubbed  $\text{Ab}^1$ ) crystallized under many different conditions and had a shallow binding site. The other free isomer ( $\text{Ab}^2$ ) crystallized in only one, high-water-exclusion condition and had a deeper binding site that was closer to the final, high-affinity complexes (7). Structural similarities between the  $\text{Ab}^2$  free form and the  $\text{Ab}^3\text{-L}$  complexes led us to postulate that it is  $\text{Ab}^2$  rather than  $\text{Ab}^1$  that is the binding isomer. However, in the absence of an encounter complex structure this could not be proved. Furthermore, as with any antibody (17, 18), or protein (4), in the absence of the structure of the encounter complex, the conformational changes between the encounter and the final complex can only be assumed. To provide the missing link in the reaction pathway and precisely define the structural changes that occur after the formation of the encounter complex, we solved the structure of SPE7 in complex with anthrone.

We crystallized the  $\text{Ab}^2$ -anthrone complex under similar high-solvent-exclusion conditions as the free  $\text{Ab}^2$  isomer (Table 2). The possibility that the anthrone complex is a crystallization artifact can be ruled out largely because it also has the same crystal contacts, lattice, cell dimensions, and space group as the  $\text{Ab}^2$  structure. There is only a single packing contact involving H3 in the anthrone structure and none involving L3 residues, demonstrating that packing does not affect the conformation of the binding site in the encounter complex or in free isomer  $\text{Ab}^2$ . The anthrone complex superposes on the free  $\text{Ab}^2$  structure with an rms deviation of 0.34  $\text{\AA}$  for the entire structure and 0.12  $\text{\AA}$  for the scaffold only. In both structures, the binding site is funnel-shaped with an opening between the H3 and L3 loops (Fig. 3). The anthrone ligand stacks against the side chain of Trp-L93 from the L3 loop, with its single oxygen pointing toward the H1 and H2 CDR loops. The same

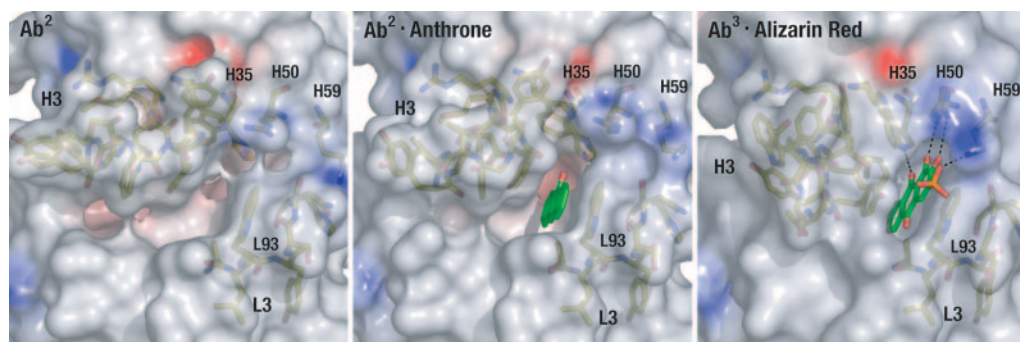


**Fig. 3.** The binding-site conformations of SPE7. The semitransparent surface view is colored by electrostatic potential (blue for positive, red for negative). Noted are light-chain (L) and heavy-chain (H) CDR3 loops and residues that play a key role in ligand binding. The free antibody isomer  $\text{Ab}^2$  1OCW (7) forms a nonspecific encounter complex with a range of ligands, as can be seen in the  $\text{Ab}^2$ -anthrone structure 1BJM. The latter isomerizes to give the final, high-affinity complex  $\text{Ab}^3$ -alizarin red 1OAR (see also Movie 3). The ligands stacks against L3 residue Trp-93 in both the  $\text{Ab}^2$  and  $\text{Ab}^3$  complexes, but anthrone makes no hydrogen bonds with  $\text{Ab}^2$ . In contrast, alizarin red makes a number of hydrogen bonds to  $\text{Ab}^3$ .

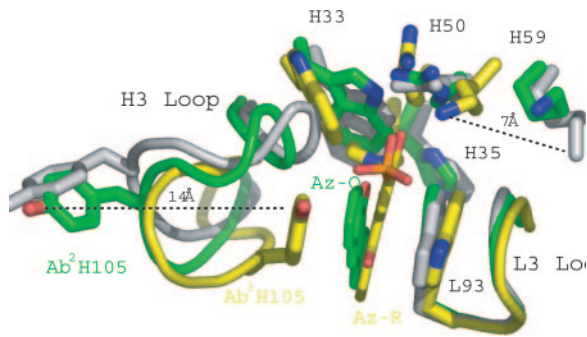


**Fig. 4.** Superposition of H3 loops at different stages of ligand complexation. Shown are CDR loops and side chains for Ab<sup>2</sup> (gray), Ab<sup>2</sup>-anthrone (green), and Ab<sup>3</sup>-alizarin red (yellow). Although the Ab<sup>2</sup> and Ab<sup>2</sup>-anthrone structures vary only slightly (Movie 1), the formation of the final high-affinity complex (Ab<sup>3</sup>-alizarin red) is accompanied by significant conformational change, in particular of the H3 loop (Movie 3).

Trp-L93 orientation is seen in Ab<sup>2</sup> and in the high-affinity complex Ab<sup>3</sup> (but not in the nonbinding free isomer Ab<sup>1</sup>). Stacking of anthrone against Trp-L93 is also consistent with the large drop in fluorescence that accompanies formation of the encounter complex in solution (Fig. 1A). Thus, both kinetics and structural data indicate that we have captured the structure of an on-pathway intermediate. To assess the subtle conformational differences between the two structures, we used adiabatic mapping software (19). Briefly, a restrained interpolation is created by generating a number of energy-minimized intermediates. The resulting “morph” or movie illustrates which parts of the Ab<sup>2</sup> structure are altered after complex formation and how these changes could plausibly take place. As can be seen in Movie 1, which is published as supporting information on the PNAS web site, the exchange between Ab<sup>2</sup> and the Ab<sup>2</sup>-anthrone complex involves “flexing,” or “breathing,” of the H3 loop (20). This subtle movement is in contrast with the isomerization of the two free forms, Ab<sup>1</sup> and Ab<sup>2</sup>, where large conformational changes of CDR loops L3 and H3 completely alter the binding site topography (Movie 2, which is published as supporting information on the PNAS web site).

**Isomerization to the Final High-Affinity Complex.** The pocket observed in both Ab<sup>2</sup> and Ab<sup>2</sup>-anthrone is also present in the high-affinity complexes (Ab<sup>3</sup>-L) such as the alizarin red complex shown (Fig. 3). The benzene rings of the anthrone in the encounter complex structure and those of alizarin red in the Ab<sup>3</sup>-L complex superpose closely, suggesting that the high-affinity ligands do not move after their initial capture. Furthermore, alizarin red can be docked into the anthrone structure without steric clash, confirming that the ligands share the same encounter complex. However, there are considerable structural differences in the antibody-binding site between the encounter complex and high-affinity structure, primarily in the H3 loop. In the high-affinity complex, the H3 loop has swung into the binding site to completely enclose the ligand and seal off the open end of the funnel. This movement brings Tyr-H105 to stack against the alizarin red ligand such that it is sandwiched between it and Trp-L93. The final C<sup>α</sup> position of H105 differs by >6 Å from the encounter complex, whereas its side chain moves over 14 Å (Fig. 4). The magnitude of this change (and others involving side chains from H1 and H2) is illustrated in Movie 3, which is published as supporting information on the PNAS web site.

The structural differences between the Ab<sup>2</sup>-L and Ab<sup>3</sup>-L complexes account for the >1,000-fold increase in affinity that is ascribed to their isomerization in the kinetic model (Scheme 1) and further support our assignment of the anthrone complex as an on-pathway intermediate. The anthrone ligand in the Ab<sup>2</sup> complex is highly solvent-exposed, whereas in the Ab<sup>3</sup> complex alizarin red

is almost entirely buried. Shape complementarity statistics (Sc) (21) show that anthrone exhibits good complementarity with the light chain of Ab<sup>2</sup> (Sc = 0.85; 1 being a precise fit) but poor complementarity with the heavy chain (0.51). In contrast, alizarin red binds Ab<sup>3</sup> with an Sc of >0.8 for both chains. The Sc scores underline the fact that initial capture of ligands is accomplished by the light chain (specifically Trp-L93) but that specificity and high affinity are encoded by conformational rearrangement of the heavy-chain loops. The key to ligand entrapment of the high-affinity complex Ab<sup>3</sup> is the ability to form specific hydrogen bonds (Fig. 3 and 4). Anthrone has reduced hydrogen-bonding potential with respect to alizarin red, but we have shown previously that ligands that have the same hydrogen-bonding potential and differ only in the position of a single hydroxyl fail to form high-affinity complexes (12). Thus, although there are only minimal requirements for encounter complex formation, formation of the high-affinity complex depends on precise stereochemistry. Conversely, the open conformation of the encounter complex explains why all ligands initially bind with the same affinity. When docked into the anthrone structure, alizarin red loses its ability to hydrogen bond, because the hydrogen-bonding residues in Ab<sup>3</sup> are inaccessible. Superposition of the complexed structures show that these residues are the focus of the induced-fit change, which correlates with the pre-steady-state kinetics in which the induced-fit step displays the smallest fluorescence change, indicating that residues other than the central Trp-L93 are involved. In the Ab<sup>3</sup> complex, the NZ atom of Lys-H59 moves ≈7 Å to form a hydrogen bond with one of the sulfate oxygen atoms of alizarin red (Fig. 4). Arg-H50 rearranges to place its NE and NH1 atoms within hydrogen-bond distance of the ligand’s hydroxyl oxygens. Finally, Trp-H33 is rotated out of the binding site and replaced with the side chain of His-H35, allowing the histidine NE2 atom to hydrogen bond with the carbonyl oxygen of alizarin red. Together, the kinetics and the structure of the encounter complex reveal that ligand binding is mediated by a process of indiscriminate capture, followed by a precise read-out of specificity.

## Discussion

Induced fit is a commonly invoked mechanism not only in antibody-antigen binding (22, 23) but in all other protein-ligand interactions, in particular when structural differences are observed between the complexed and free forms. Yet, this mechanism presumes the existence of intermediates that are rarely established in a direct manner. Presented here is the structure of a transient antibody-encounter complex. This structure has allowed us to dissect the order in which structural changes take place during binding and determine how SPE7 can be both promiscuous and specific.

We previously hypothesized that SPE7 must have a mechanism to discriminate between ligands, which we referred to as “kinetic proofreading” (7). However, proofreading is normally applied to those processes in which energy is expended between individual binding steps. Discrimination in SPE7 arises from a combination of a prebinding isomerization (Ab<sup>1</sup> ↔ Ab<sup>2</sup>; Scheme 1) and a slow postbinding isomerization (Ab<sup>2</sup>-L ↔ Ab<sup>3</sup>-L). This mechanism is reminiscent of the kinetic discrimination mechanism observed in the *Tetrahymena* ribozyme, in which slow formation of a catalytically active guanosine complex prevents catalysis of nonspecific substrates (10). In SPE7, the catalytically active complex is represented by a high-affinity conformation (Ab<sup>3</sup>) in which hydrogen-bond partners are accessible. The promiscuous Ab<sup>2</sup> isomer allows rapid sampling of a wide range of compounds, but the effective affinity of the resulting complex is reduced by a fast dissociation rate ( $k_{-2}$ ), because of the lack of hydrogen-bond partners, and by the competition with a more stable nonbinding isomer (Ab<sup>1</sup>). The dissociation rate ( $k_{-2}$ ) and the isomerization rate ( $k_{-1}$ ) are of very similar magnitude (≈100 and ≈60 s<sup>-1</sup>, respectively; see Table 1), which suggests that these events are kinetically coupled. Specific ligands achieve a dramatic increase in affinity by locking the antibody in a new conformation in which the heavy-chain loops are

rearranged to permit specific hydrogen bonds. In SPE7, the fact that isomerization to this high-affinity form is slow means that only specific ligands accumulate. In this way, SPE7 can take highly related ligands that initially bind with the same affinity and introduce a discrimination factor of >1,000-fold.

This kinetic discrimination mechanism has several interesting facets. The forward isomerization rate ( $\text{Ab}^2\text{-L} \rightarrow \text{Ab}^3\text{-L}$ ) seems to be quite slow ( $t_{1/2} \approx 0.5$  s), but the reverse rate must be even slower ( $t_{1/2} > 10$  min). Thus, fidelity of binding is ensured at the cost of slow association. In fact, because dissociation from the  $\text{Ab}^2\text{-L}$  encounter complex ( $t_{1/2} \approx 7$  ms) is much faster than the forward isomerization rate, even when specific ligands are bound,  $\text{Ab}^3\text{-L}$  is trapped only once in 150 encounters (on average). The likelihood of a nonspecific ligand becoming trapped is effectively zero. Second, the relaxation rates for the isomerization of the complexes with DNP-Ser, alizarin red ( $k_3 + k_{-3}$ ), and furazolidone seem to be similar despite large differences in the structures and affinities of these ligands (see Table 1). The similarity of rates suggests that the conformational rearrangement between  $\text{Ab}^2\text{-L}$  and  $\text{Ab}^3\text{-L}$  is an intrinsic property of the antibody, and the ligands do not induce or accelerate the isomerization. The latter is obviously a hypothesis that can be confirmed only after the direct measurement of the isomerization rates ( $k_3$  and  $k_{-3}$ ). Third, it is clear that a dramatic increase in affinity could be achieved by stabilizing  $\text{Ab}^3$  to obtain a lock-and-key binding mode. This route may represent a common strategy in affinity maturation, although other routes certainly exist (24). It has been shown that matured antibodies with higher affinity are also more rigid than their germ-line precursors (20, 25, 26).

Furthermore, Foote and Milstein (27) demonstrated that affinity-matured antibodies have faster on rates. It is curious that on rates seem to be more important than off rates in terms of antigen clearance (28), which argues that affinity improvement through on-rate increase is particularly important. The apparent on rate of SPE7 is quite slow. An increase in the rates of isomerization ( $\text{Ab}^1 \leftrightarrow \text{Ab}^2$  and  $\text{Ab}^2\text{-L} \rightarrow \text{Ab}^3\text{-L}$ ) would increase the apparent on rate but would also increase the cross-reactivity of SPE7. The affinity toward nonspecific ligands would increase along with the specific ligands, and thus nonspecific ligands (were they to have an *in vivo* relevance) could trigger a biological response (e.g., allergy or autoimmunity).

The phenomenon of conformational diversity, kinetic discrimination, and affinity maturation seem to be strongly interconnected. The existence of multiple isomers can be beneficial by increasing the repertoire of the immune response (16). Multiple conformational states also provide a gating mechanism to distinguish between structurally related ligands. In a wider context, kinetic discrimination mechanisms may also apply to other protein–ligand recognition events as well as RNA–ligand interactions (10). A model in which structural dynamism is linked to recognition specificity could explain, for example, how proteins bind multiple ligands in a specific manner and how others, although capable of binding many ligands, are activated by only a few.

We are grateful to Asael Herman for his insightful suggestion and to Greg Winter for his ongoing support. Financial support by the Wellcome Trust and the Israel Science Foundation is gratefully acknowledged. D.S.T. is the incumbent of the Elaine Blond Career Development Chair.

- Mason, D. (1998) *Immunol. Today* **19**, 395–404.
- Kriwacki, R. W., Hengst, L., Tennant, L., Reed, S. I. & Wright, P. E. (1996) *Proc. Natl. Acad. Sci. USA* **93**, 11504–11509.
- Sprang, S. R. (1997) *Annu. Rev. Biochem.* **66**, 639–678.
- Goh, C. S., Milburn, D. & Gerstein, M. (2004) *Curr. Opin. Struct. Biol.* **14**, 104–109.
- De Guzman, R. N., Martinez-Yamout, M. A., Dyson, H. J. & Wright, P. E. (2004) *J. Biol. Chem.* **279**, 3042–3049.
- Holler, P. D. & Kranz, D. M. (2004) *Mol. Immunol.* **40**, 1027–1031.
- James, L. C., Roversi, P. & Tawfik, D. S. (2003) *Science* **299**, 1362–1367.
- Wright, P. E. & Dyson, H. J. (1999) *J. Mol. Biol.* **293**, 321–331.
- Del Carmine, R., Molinari, P., Sbraccia, M., Ambrosio, C. & Costa, T. (2004) *Mol. Pharmacol.* **66**, 356–363.
- Karbstien, K. & Herschlag, D. (2003) *Proc. Natl. Acad. Sci. USA* **100**, 2300–2305.
- Varga, J. M., Kalchschmid, G., Klein, G. F. & Fritsch, P. (1991) *Mol. Immunol.* **28**, 641–654.
- James, L. C. & Tawfik, D. S. (2003) *Protein Sci.* **12**, 2183–2193.
- Collaborative Computational Project, Number 4 (1994) *Acta Crystallogr. D* **50**, 760–763.
- DeLano, W. L. (2002) The PYMOL Molecular Graphics System (DeLano Scientific, San Carlos, CA).
- Fersht, A. (1985) *Enzyme Structure and Mechanism* (Freeman, New York).
- Foote, J. & Milstein, C. (1994) *Proc. Natl. Acad. Sci. USA* **91**, 10370–10374.
- Sundberg, E. J. & Mariuzza, R. A. (2002) *Adv. Protein Chem.* **61**, 119–160.
- Rini, J. M., Schulze-Gahmen, U. & Wilson, I. A. (1992) *Science* **255**, 959–965.
- Krebs, W. G. & Gerstein, M. (2000) *Nucleic Acids Res.* **28**, 1665–1675.
- Jimenez, R., Salazar, G., Yin, J., Joo, T. & Romesberg, F. E. (2004) *Proc. Natl. Acad. Sci. USA* **101**, 3803–3808.
- Lawrence, M. C. & Colman, P. M. (1993) *J. Mol. Biol.* **234**, 946–950.
- Stanfield, R. L., Takimoto-Kamimura, M., Rini, J. M., Profy, A. T. & Wilson, I. A. (1993) *Structure (London)* **1**, 83–93.
- Wilson, I. A. & Stanfield, R. L. (1994) *Curr. Opin. Struct. Biol.* **4**, 857–867.
- Li, Y., Li, H., Yang, F., Smith-Gill, S. J. & Mariuzza, R. A. (2003) *Nat. Struct. Biol.* **10**, 482–488.
- Jimenez, R., Salazar, G., Baldrige, K. K. & Romesberg, F. E. (2003) *Proc. Natl. Acad. Sci. USA* **100**, 92–97.
- Manivel, V., Sahoo, N. C., Salunke, D. M. & Rao, K. V. S. (2000) *Immunity* **13**, 611–620.
- Foote, J. & Milstein, C. (1991) *Nature* **352**, 530–532.
- Roost, H. P., Bachmann, M. F., Haag, A., Kalinke, U., Pliska, V., Hengartner, H. & Zinkernagel, R. M. (1995) *Proc. Natl. Acad. Sci. USA* **92**, 1257–1261.